Journal of Nanobiotechnology

RESEARCH

Open Access

Lymph node metastasis diagnosis of postoperative OSCC patients by analyzing extracellular vesicles in drainage fluid based on microfluidic isolation

Zi-Zhan Li[1], Ze-Min Cai[1], Wen-Tao Zhu[2], Nian-Nian Zhong[1], Lei-Ming Cao[1], Guang-Rui Wang[1], Yao Xiao[1], Zhao-Qi Zhu[1], Xuan-Hao Liu[1], Ke Wu[5], Rong-Xiang He[3], Xing-Zhong Zhao[5], Bing Liu[1,4*], Bo Cai[2*] and Lin-Lin Bu[1,4,5*]

Abstract

Lymph node metastasis (LNM) is a typical marker in oral squamous cell carcinoma (OSCC) indicating poor prognosis. Pathological examination by artificial image acquisition and analysis, as the main diagnostic method for LNM, often takes a week or longer which may cause great anxiety of the patient and also retard timely treatment. However, there are few efficient fast LNM diagnosis methods in clinical applications currently. Our previous study profiled the proteomics of extracellular vesicles (EVs) derived from postoperative drainage fluid (PDF) and showed the potential of detecting specific EVs that expressed aspartate β-hydroxylase (ASPH) for LNM diagnosis in OSCC patients. Considering that the analysis of $ASPH^+$ PDF-EVs is challenging due to their low abundance (counting less than 10% of total EVs in PDF) and the complex EV isolation process of ultra-centrifugation, we developed a facile platform containing two microfluidic chips filled with antibody-modified microbeads to isolate $ASPH^+$ PDF-EVs, with both the capture and retrieval rate reaching around 90%. Clinical sample analysis based on our method revealed that a mean of 6×10^6 /mL $ASPH^+$ PDF-EVs could be isolated from LNM^+ OSCC patients compared to 2.5×10^6 /mL in LNM^- OSCC ones. When combined with enzyme-linked immunosorbent assay (ELISA) technique that was commonly used in clinical laboratories in hospitals, this microfluidic platform could precisely distinguish postoperative OSCC patients with LNM or not in several hours, which were validated by a double-blind test containing 6 OSCC patients. We believe this strategy has promise for early diagnosis of LNM in postoperative OSCC patients and finally helps guiding timely and reasonable treatment in clinic.

Keywords Extracellular vesicles, Postoperative drainage fluid, Microfluidics, Lymph node metastasis, Oral squamous cell carcinoma

*Correspondence:
Bing Liu
liubing9909@whu.edu.cn
Bo Cai
bcai@jhun.edu.cn
Lin-Lin Bu
lin-lin.bu@whu.edu.cn

Full list of author information is available at the end of the article

Introduction

Lymph node metastasis (LNM) indicates poor prognosis in oral squamous cell carcinoma (OSCC) [1], which are closely associated with high mortality rate of OSCC [2, 3]. The diagnosis of LNM typically relies on postoperative pathological examination [4] and often takes a week or even longer [5]. This long period time of delayed diagnosis, however, leads to significant challenges for disease management. At first, postoperative OSCC patients frequently endure significant psychological burdens when they wait for diagnostic results [6, 7]. This psychological quagmire, with manifestations ranging from depression to self abandonment, may foster an antagonistic stance towards therapeutic interventions, and thus compromising on patient healthcare and augmenting extra tasks of medical professionals [8, 9]. Moreover, the emotional distress is also a precipitating factor in suicides among postoperative OSCC patients in an intricately-intertwined manner [10]. Secondly, it is of great benefits to apply timely interventions or treatments such as radiotherapy or chemotherapy when LNM in postoperative OSCC happens [11, 12]. An expeditious and unambiguous diagnosis can serve as a cornerstone for orchestrating a seamless multidisciplinary treatment paradigm, therefore navigating complex therapeutics with sufficient precision and ultimately enhancing the clinical healthcare and outcomes for postoperative OSCC patients [13]. Therefore, fast diagnosis of LNM for postoperative OSCC patients greatly facilitates appropriate strategies for both psychological and pathological intervention and thus can significantly improve the prognosis and life quality of OSCC patients [14, 15]. However, previous efforts such as combining artificial intelligence (AI) with imaging technology to fast diagnose LNM [16] face challenges relating to poor accuracy and reliability [17].

Liquid biopsy is increasingly employed in cancer molecular analysis, thereby facilitating the implementation of precise oncology approaches [18]. Liquid biopsy surpasses traditional imaging modalities in the diagnosis of both early-stage cancer and occult LNM, demonstrating notable virtues [19, 20]. It not only circumvents radiation exposure but also exhibits favorable economic feasibility. Furthermore, its capability for serial assessment facilitates tracking treatment dynamics and prognostic forecasting in LNM, thereby optimizing clinical care for LNM patients [21]. Extracellular vesicles (EVs) are cell-secreted tiny spheres carrying various biomolecules such as proteins, lipids, DNA and RNA, which play a critical role in mediating intercellular communication [22]. In tumor microenvironment, abundant cancer-related EVs that contain information of cancer progression and metastasis are released into biofluids by the primary tumor [23]. Therefore, liquid biopsy based on EVs from peripheral blood or other body fluids is emerging as a fast, convenient and non-invasive technology for early diagnosis and precise prognosis of various cancers [20]. Recent studies demonstrate that tumor cell-derived EVs promote metastasis to sentinel lymph nodes and showed the potential of EV analysis for diagnosing LNM, for example, high levels of miRNA-21 and lncRNA in serum-derived exosomes can reflect LNM of laryngeal squamous cell carcinoma [24]. Our previous study characterized the protein profile of EVs collected from the postoperative drainage fluid (PDF) of OSCC patients after neck dissection [25]. Results revealed the distinct difference of PDF-EVs protein expression between OSCC patients with/without LNM, validating that some specific PDF-EVs can be an indicator for LNM in OSCC. Conventionally, PDF is usually discarded as medical waste despite of its large volume and easy access [26], but our research unearths its diagnostic and predictive value in providing EVs that comprise abundant LNM information.

However, a major challenge in analyzing EVs from PDF for clinical LNM diagnosis lies in the limited abundance of specific EVs [27]. Traditional EV isolation methods include ultra centrifugation (UC) [28], differential ultra centrifugation (dUC) and membrane filtration [29], all of which suffer from low efficiency and poor selectivity [30]. With the advantage of precisely manipulating a trace of liquid, the fast-developing technique of microfluidics becomes a powerful tool for EV isolation, purification and analysis from various kinds of body fluids [31, 32]. Herein, we introduce a microfluidic platform utilizing antibody-grafted microbeads to isolate and purify EVs that highly express aspartate β-hydroxylase (ASPH) from neck dissection PDF of OSCC patients, which shows the potential for fast LNM diagnosis in postoperative OSCC patients (Fig. 1). At first, ASPH expression of PDF-EVs was confirmed to correlate with LNM in OSCC through database investigation, bioinformatic analysis and pathological assays. To isolate PDF-EVs, 10 μm silica (SiO_2) microbeads grafted with anti-EpCAM (epithelial cell adhesion molecule) and anti-ASPH were loaded in two microfluidic chips, respectively, and filtrated by micropillar arrays inside the chips. When PDF collected from OSCC patients flowed through the chips, $ASPH^+$ PDF-EVs could be captured and purified by the immuno-affinity of those antibody-modified microbeads through the chip cascades, subsequently released due to the fluidic hydrodynamics and pH variation, and finally collected for downstream analysis of imaging and bioassays. As a proof of concept showing clinical practice, PDF from OSCC patients with/without LNM were blind-treated. Results validated the potential of our strategy for predicting LNM risk in postoperative OSCC patients, demonstrating its ability in guiding timely and precise treatment of OSCC patients.

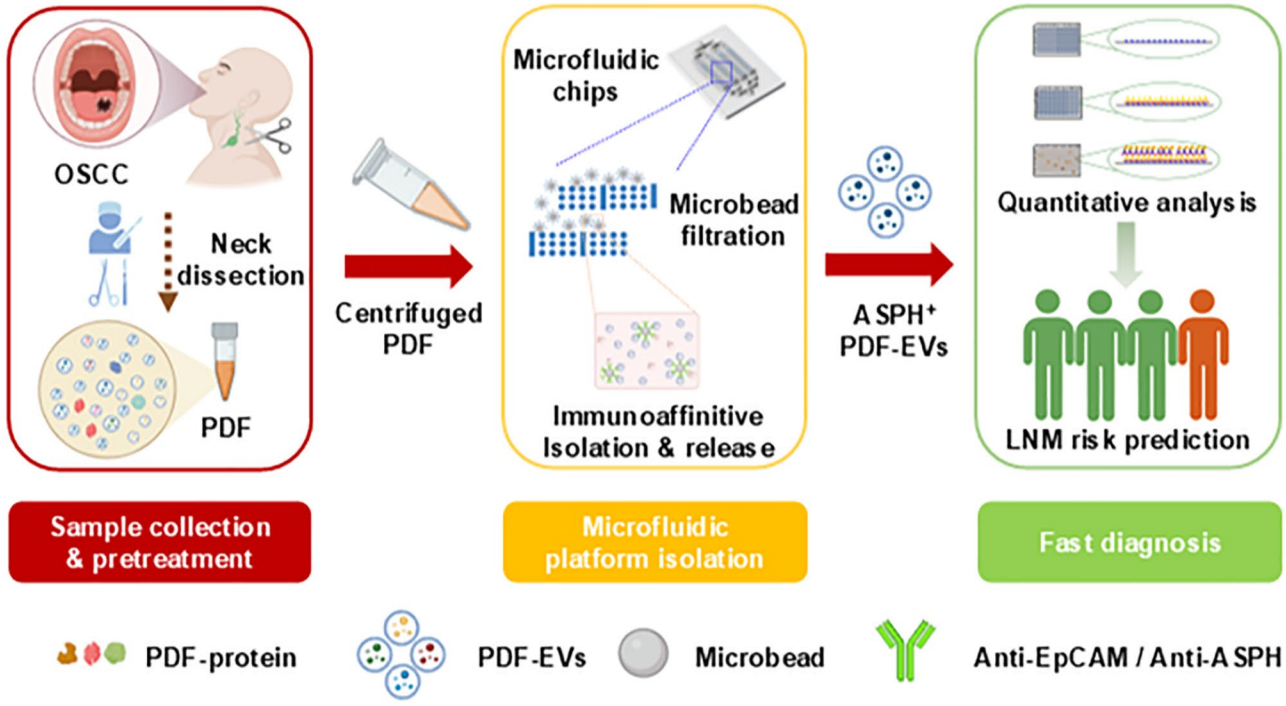

Fig. 1 Schematic of diagnosing LNM in postoperative OSCC patients by PDF-EV analysis based on microfluidic isolation using antibody-grafting microbeads. PDF is collected after neck dissection and ASPH$^+$ PDF-EVs are isolated and purified through microbead-based immuno-affinity capture and release in microfluidic chips. Subsequent ELISA analysis of ASPH$^+$ PDF-EVs enables fast diagnosis of LNM risk in postoperative OSCC patients. LNM, lymph node metastasis; OSCC, oral squamous cell carcinoma; PDF, postoperative drainage fluid; EVs, extracellular vesicles; ASPH, aspartate β-hydroxylase; ELISA, enzyme-linked immunosorbent assay

Experimental section

Proteomic analysis of EVs using liquid chromatography-mass spectrometry/mass spectrometry (LC-MS/MS)

The proteomic profiles of the PDF-EVs were determined by Wuhan GeneCreate Biological Engineering Co., Ltd. For more detailed information, please refer to our previous work [25].

Evaluation of EV isolation by antibody-grafted microbeads

At first, the cell culture medium or PDF obtained from patients was pre-centrifuged to remove potential cells or cellular debris. Subsequently, 0.1 g of the as-prepared antibody-grafted microbeads was added into the supernatant of the cell culture medium or PDF, stirred and incubated for one hour to bond specific EVs. After then, the microbeads were collected by gentle centrifugation and washed with PBS for 3 times. To release the captured EVs from the surface of the microbeads, glycine-HCl was added into the suspension of the EVs-microbeads complex at the final concentration of 0.1 M, and then 1 M Tris-HCl was added dropwise to set the pH value at 7.4 for the final solution. After removing the microbeads by gently centrifuging, the suspension containing target EVs was obtained.

Evaluation of EV isolation by the microfluidic chips

Before implementing EV isolation, all the microfluidic chips were rinsed with phosphate buffer saline (PBS) for 3 times using syringe pumps (TS-1 A, Longer, China) with flow rate of 1 mL/min, and then the microchips were filled with PBS to carefully remove air bubbles, especially those existing among the micropillars. Next, 0.1 g of the antibody-grafted microbeads were suspended in the mixture of PBS and glycerol with the volume ratio of 1:1, injected into the microchips with the flow rate of 200 μL/min and immobilized by the micropillar arrays. After then, 1 mL PBS was pumped into the microchips at 200 μL/min to remove residual glycerol.

Subsequently, 1 mL prepared samples (the pretreated cell culture medium or PDF) were injected into the microfluidic chips at different flow rates using syringe pumps. When EV isolation finished, the microchannels were washed with 1 mL PBS at the flow rate of 200 μL/min to remove excessive sample solution. To release EVs from the filtered microbeads inside the microchips, 1 mL 0.1 M glycine-HCl solution was pumped into the microchips at different flow rates, and the solution was collected into a tube and the pH value was set at 7.4 by adding 1 M Tris-HCl. For isolating ASPH$^+$ PDF-EVs, this isolation process was repeated successively using two microfluidic chips filling with anti-EpCAM-grafted

microbeads and anti-ASPH-grafted microbeads, respectively.

Statistical analysis

All statistical analyses were performed using GraphPad Prism 8.0 software. Two-tailed unpaired t-tests were used to analyze between two groups. One-way ANOVA analysis of variance was used to analyze multiple groups. All results are presented as mean ± SEM. The Tukey's post-hoc test was used following ANOVA. Statistical significance was set at $P<0.05$.

Results and discussion

ASPH$^+$ PDF-EVs as a predictor for LNM in OSCC

ASPH is a type II transmembrane protein that can promote cancer progression and metastasis by inducing the formation of cancer stem cells, and it has been considered as a potential therapeutic target for various cancers [33, 34]. After analyzing the data of OSCC patients from the public database The Cancer Genome Atlas (TCGA) using bioinformatic methods, it was found that mRNA level of ASPH in OSCC tissues was significantly higher than that in adjacent tissues (Fig. 2A). Further investigation showed that OSCC patients with highly-expressed ASPH had a lower survival rate compared to those without significant ASPH expression (Fig. 2B). Given the fact that LNM indicated poor prognosis in OSCC patients [35], we speculated that ASPH expression was probably correlated with LNM. For validation, tissue samples from OSCC patients with/without LNM, respectively were collected and immunohistochemically stained. As shown in Fig. 2C, it could be seen that ASPH expression in the

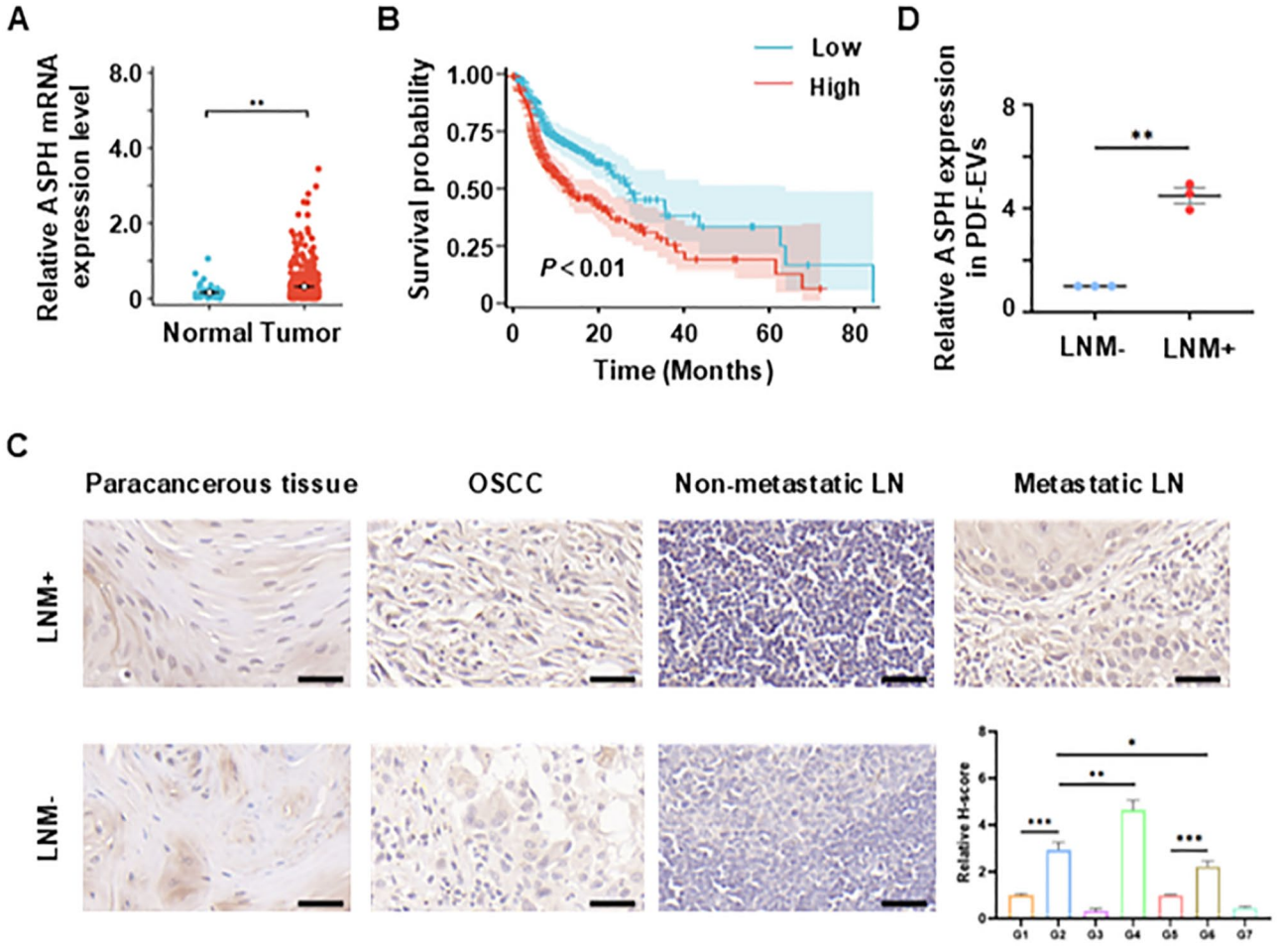

Fig. 2 ASPH$^+$ PDF-EVs as a predictor for LNM in OSCC. (**A**) ASPH expression in OSCC tumor tissue is significantly higher than in normal tissue. (**B**) High ASPH expression predicts a shorter survival duration for OSCC patients. (**C**) ASPH is highly expressed in metastatic LN and primary lesions with metastasis, while its expression is significantly lower in adjacent cancerous tissues and normal lymph nodes. Scale bar, 20 μm. G1, LNM+ / paracancerous tissue; G2, LNM+ / OSCC; G3, LNM+ / Non-metastatic LN; G4, LNM+ / Metastatic LN; G5, LNM- / paracancerous tissue; G6, LNM- / OSCC; G7, LNM- / Non-metastatic LN. (**D**) Protein mass spectrometry analysis revealed that the ASPH expression level in PDF-EVs from OSCC patients with LNM was higher than that from OSCC patients without LNM. *P<0.05, **P<0.01, ***P<0.001. ASPH, aspartate β-hydroxylase; PDF, postoperative drainage fluid; EVs, extracellular vesicles; LNM, lymph node metastasis; LNM, lymph node metastasis; OSCC, oral squamous cell carcinoma

primary lesion of metastatic patients was higher than that of non-metastatic patients, and interestingly, ASPH expression in metastatic lymph nodes was also higher than that in the primary lesion. All the results indicated a correlation between high ASPH expression and poor prognosis of OSCC such as LNM. In our past study [25], proteomic analysis revealed that PDF-EVs had significant difference in protein expression between patients with/without LNM (Figure S1) and corresponding volcano plot demonstrated that ASPH expression in PDF-EVs was significantly higher in OSCC patients with LNM compared to patients without LNM (Figure S2). Both the analysis inferred that PDF-EVs highly expressing ASPH were expected to indicate LNM, which was further validated by examining the ASPH expression in EVs that were isolated from PDF of typical OSCC patients with/without LNM, respectively (Fig. 2D). Therefore, $ASPH^+$ PDF-EVs is experted as a key role for predicting potential LNM through a non-invasive liquid biopsy manner.

Capture and release of ASPH+ PDF-EVs using antibody-grafted microbeads

Due to the low abundance and extremely tiny size, directly isolating EVs from PDF was very challenging [36]. In this work we employed antibody-grafted microbeads as the core isolation components to specifically capture EVs through the antigen-antibody immunoaffinity (Fig. 3A). These microbeads with the diameter of 10 μm (Figure S3) were chemically modified with streptavidin for grafting biotinylated anti-EpCAM or anti-ASPH according to our previous work [37, 38]. EpCAM is highly expressed on the surface of most EVs and thus is used as a typical surface marker for separating EVs [27]. Therefore, we firstly utilized anti-EpCAM to enrich EVs and exclude potential interference such as debris in PDF. Anti-ASPH was used to further isolate specific $ASPH^+$ EVs. It was noteworthy that by rinsing the modified microbeads with 0.1 M glycine-HCl (pH=3.0), EVs could effectively detach from the microbead surface [30]. After neutralized at pH=7.4 by using 1 M Tris-HCl (pH=9.0), the released EVs were able to be retrieved without damage. As shown by scanning electron microscopy (SEM) in Fig. 3B, corresponding PDF-EVs could be effectively captured on the surface of anti-EpCAM or anti-ASPH modified microbeads, and after treated by glycine-HCl, most of the attached PDF-EVs could be released from the microbeads, whether they were immuno-bonded by anti-EpCAM or anti-ASPH.

To further verify PDF-EVs, TEM, NTA and western blot were implemented on the released EVs after microbead-based EV isolation. It could be observed that the morphology of PDF-EVs kept sphere (Fig. 3C), which was consistent with our previous description [25]. NTA measurement showed that the particle size of the released PDF-EVs mainly distributed in the range of 95–115 nm, and we inferred that the 196 nm region was mainly attributed to the influence of aggregation (Fig. 3D). Using western blotting, we investigated the characteristic proteins of the collected samples (from clinical PDF and the supernatant of SCC-9 cell line, respectively) after release treatment (Fig. 3E). The results showed that ALIX and CD9, the markers of EVs, were observed in both SCC-9 and PDF samples, while cell markers of GM130 and Calnexin did not exist in both two samples, indicating that the isolated spheres by the immuno-microbeads were EVs rather than cell debris.

Utilizing NTA for measuring the quantity of EVs in various solutions, the efficiency of those antibody-modified microbeads for capturing and releasing EVs could be calculated as following:

Capture rate = (number of EVs in original PDF – number of EVs left after microbead isolation) / (number of EVs in original PDF) (%).
Release rate = (number of EVs released from the microbeads) / (number of EVs in original PDF – number of EVs left after microbead isolation) (%).

Herein, we employed anti-EpCAM-modified microbeads to demonstrate the ability of immuno-microbeads for capturing and releasing corresponding EVs. As shown in Fig. 3F and G, despite the fact that the concentration of microbeads varied from 1×10^4 to 1×10^7 /mL, it had impact on neither the capture nor the release rate, both of which exceeded 90%. We inferred that 1×10^4 /mL microbeads were already enough to provide sufficient surface area for grafting antibody and thus bonding almost all the EVs suspended in 1 mL PDF, and the bonding between EVs and antibody-modified microbeads could be effectively broken by glycine-HCl solution to release almost all the captured EVs on the microbeads. Given the similarity between anti-EpCAM and anti-ASPH, we regarded the anti-ASPH microbeads had the same ability for capturing and releasing $ASPH^+$ PDF-EVs. Therefore, these immuno-microbeads could function as the core component for the subsequent microfluidic $ASPH^+$ PDF-EV isolation, since that they greatly increased the surface area inside the microfluidic channels which enabled effective contact between $ASPH^+$ PDF-EVs and the isolation interfaces.

$ASPH^+$ PDF-EVs isolation and purification based on microfluidic cascades

After validating the capability of antibody-grafted microbeads for capturing and releasing $ASPH^+$ PDF-EVs, specific microfluidic chips were fabricated for further EV isolation and purification. In the microfluidic chip (Fig. 4A), there were four individual microchannels

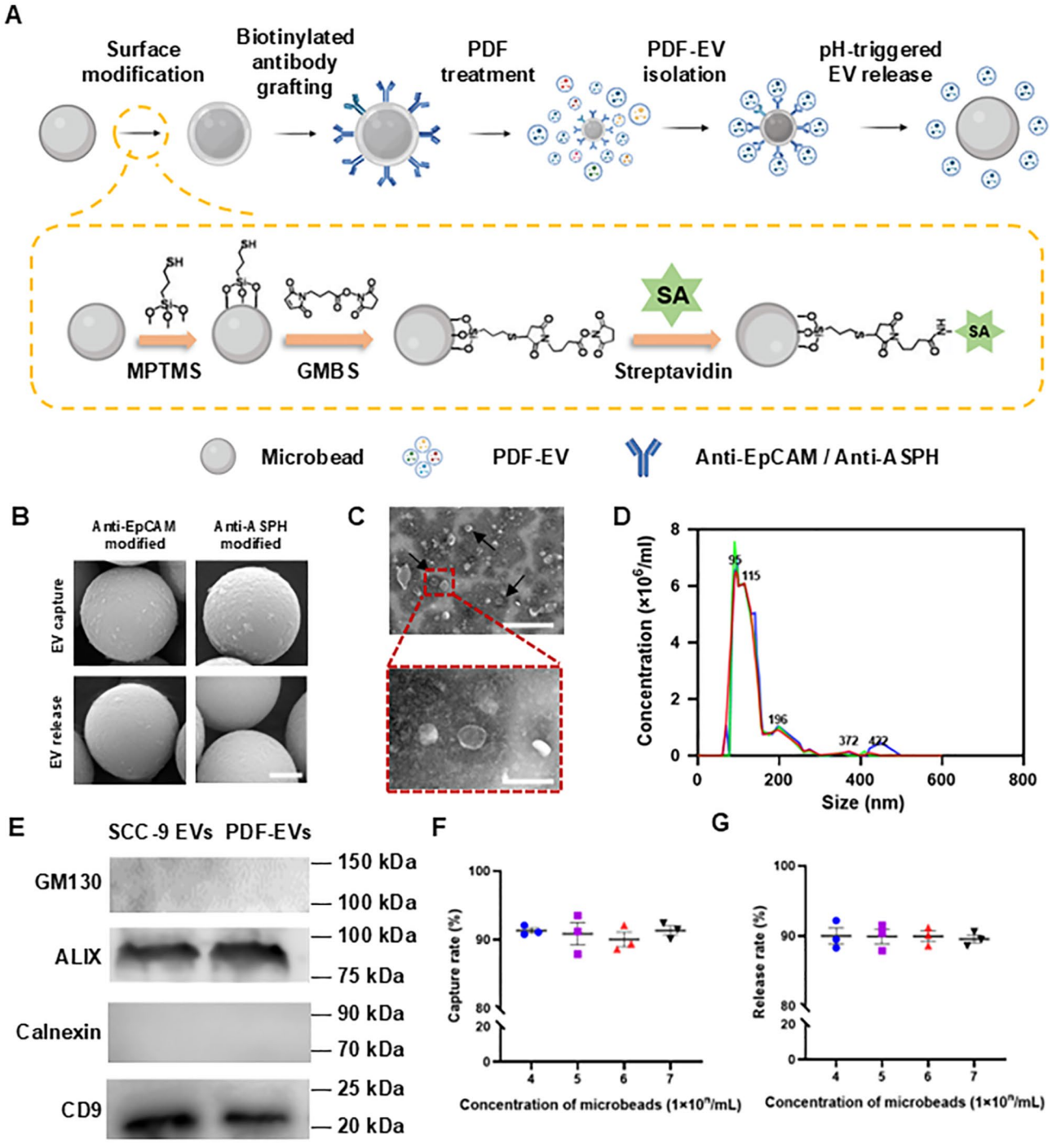

Fig. 3 Capture and release of PDF-EVs by antibody-grafted microbeads. (**A**) Schematic illustrating the working principle for the capture and release of specific PDF-EVs using antibody-modified microbeads and corresponding surface modification process. (**B**) Typical SEM images showing microbeads surface-modified with anti-EpCAM and anti-ASPH after the capture or release of corresponding PDF-EVs. Scale bars, 2 μm. (**C**) Typical TEM images depicting $ASPH^+$ PDF-EVs. Scale bars, 2 μm. (**D**) NTA analysis of EV size distribution (three times). (**E**) Western blotting analysis demonstrating the presence of EV protein markers CD9 and ALIX, as well as non-EV protein markers GM130 and Calnexin in PDF-EVs and SCC-9-EVs. (**F**) The effect of microbead concentration on EV capture rate. (**G**) The effect of microbead concentration on EV release rate. PDF, postoperative drainage fluid; EVs, extracellular vesicles; ASPH, aspartate β-hydroxylase; MPTMS, (3-mercaptopropyl) trimethoxysilane; GMBS, 4-maleimidobutyric acid N-hydroxysuccinide ester; SA, streptavidin; SEM, scanning electron microscope; TEM, transmission electron microscope; NTA, nanoparticle tracking analysis

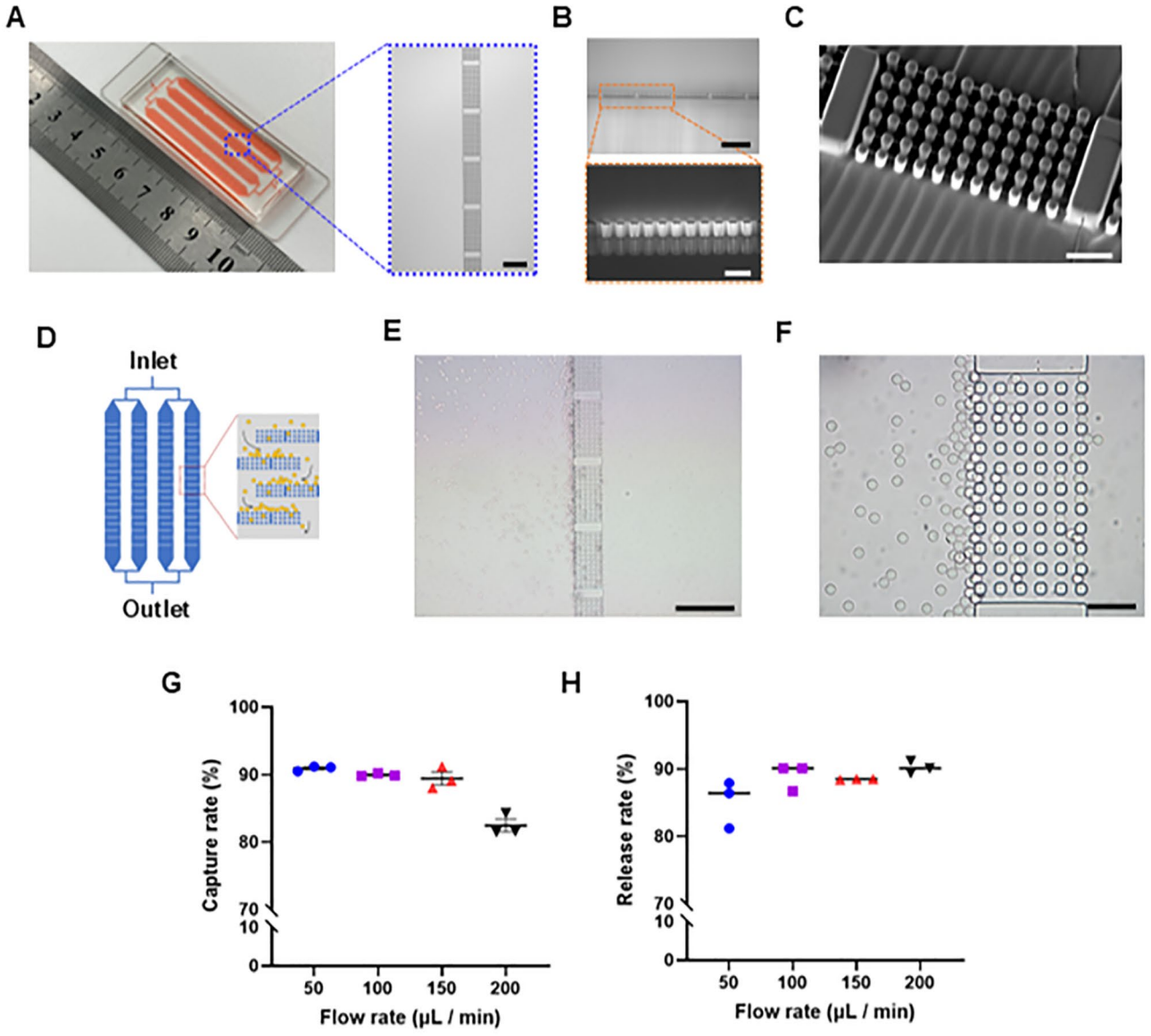

Fig. 4 ASPH$^+$ PDF-EVs isolation and purification based on microfluidic cascades. (**A**) Photographs showing the microfluidic chip in this work. The enlarged microscope image demonstrates the micropillar arrays fabricated inside the chip. Scale bar, 200 μm. (**B**) Microscope images displaying the side views of the micropillars and microchannels. Scale bars, 200 μm (top) and 50 μm (bottom). (**C**) SEM image showing a micropillar array fabricated inside the microfluidic chip. Scale bar, 50 μm. (**D**) Schematic showing the design of the microfluidic chip and the micropillar arrays that form "fences" to filter the microbeads. (**E**) The micropillar arrays play as a "fence" for filtering the microbeads. Scale bar, 200 μm. (**F**) Despite that some microbeads may pass through the micropillar arrays, they are finally filtered by downstream micropillar arrays. Scale bar, 25 μm. (**G**) The effect of flow rate on EV capture rate of the microfluidic chip. (**H**) The effect of flow rate on EV release rate of the microfluidic chip. PDF, postoperative drainage fluid; ASPH, aspartate β-hydroxylase; EVs, extracellular vesicles; SEM, scanning electron microscope

(whose width was 3530 μm and length was 4 cm) which could simultaneously treat the injected sample liquid in a parallel manner and thus increase the thoughput. Inside each microchannel, there were 19 rows of micropillar arrays (with 11×6 square micropillars (10 μm wide) in every array) to form "fences". These micropillars were as high as the microchannels (approximately 25 μm) and the distance between two adjacent micropillars was 8 μm (Fig. 4B and C). Therefore, when the 10 μm-diameter microbeads were carried downstream by the fluid flow, they were filtered by the micropillar "fences" (Fig. 4D and E) while the pure liquid could pass through the micropillar arrays (**Movie S1**). Despite that some microbeads might flow through one row of the micropillar arrays due to the high hydrodynamic force caused by fast flow rate (Fig. 4F), they would be further filtered by other downstream micropillar "fences" and thus high filling efficiency of the antibody-grafted microbeads was realized

inside the microfluidic chips. In order to ensure the sufficient capture of EVs from PDF, we filled excessive microbeads (about 10^7) inside the microfluidic chip. In order to avoid possible blocking when filling a large amount of microbeads, there was a 250 μm-wide opening for the flowing of excessive microbeads that accumulated before the micropillar "fence", as demonstrated in the inset schematic of Fig. 4D. It was noteworthy that the accumulation of the microbeads inside the microfluidic chip not only increased the surface for modifying antibodies compared to the empty microchannel, but also enhanced the mixture and vortex of the fluid flow in the microchannels that could benefit the contact and bonding between PDF-EVs and the microbeads, and thus finally improved the performance of our microfluidic platform for isolating PDF-EVs.

In order to implement the isolation and purification of $ASPH^+$ PDF-EVs, we employed a strategy using a cascade of two aforementioned microfluidic chips. The first microfluidic chip was filled by anti-EpCAM-grafted microbeads to isolate PDF-EVs, given the fact that EpCAM was the typical marker protein of EVs that was highly-expressed on the EVs surface. This process could reduce the interference of cell debris suspended in PDF. Subsequently, the first microfluidic chip was rinsed with a solution buffer (0.1 M glycine HCl (pH=3)) and the captured PDF-EVs were released and collected into a tube containing 1 M Tris-HCl (pH=9.0) to neutralize at pH 7.4. To further isolate and purify $ASPH^+$ PDF-EVs, the collected PDF-EVs were introduced into the second microfluidic chip filling with anti-ASPH-grafted microbeads. Due to the immuno-affinity between the antibody and ASPH protein expressed on the EV surface, sole $ASPH^+$ PDF-EVs could be effectively isolated and other kinds of EVs flowed away with the buffer solution. After finishing the sample treatment, $ASPH^+$ PDF-EVs could be released in the same way as aforementioned for further analysis.

To investigated the influence of different flow rates on the EV capture and release rate using microfluidic chips, we employed microfluidic chips filled by anti-EpCAM modified microbeads to isolate EVs as a proof of concept. The concentration of EVs collected from cell line samples was adjusted to $(1\pm0.05)\times10^8$/mL based on NTA measurement, and by detecting the amount of EVs in solutions collected from different ports, the EV capture and release rate of the microfluidic chip could be calculated as following:

Capture rate = (number of EVs in inlet solution – number of EVs in outlet solution) / (number of EVs in inlet solution) (%).

Release rate = (number of EVs released in outlet solution) / (number of EVs in inlet solution – number of EVs in outlet solution) (%).

Our results indicated that when the flow rate varied between 50 and 150 μL/min, the capture rate kept around 90% and changed little. However, when the flow rate increases to 200 μL/min, the EV capture rate of the microfluidic chip decreased to 82.47 ± 1.59% (Fig. 4G). This decrease could be attributed to the fact that excessively faster flow rate hindered the specific capture of EVs by the antibodies on the surface of the microbeads due to less time for affinity reactions. Subsequently, we measured the release efficiency of the captured EVs. We observed that when the flow rate of glycine-HCl solution inside the microfluidic chip varied between 50 and 200 μL/min, it did not significantly affect the EV release (Fig. 4H). Overall, we adopted the flow rate of 100 μL/min for sample injection and 200 μL/min for glycine-HCl solution, and thus costed less than half an hour when dealing with 1 mL PDF sample to collect $ASPH^+$ PDF-EVs from OSCC patients.

Evaluation of the microfluidic platforms and clinical sample analysis

To evaluate the performance of the microfluidic platform for specifically isolating $ASPH^+$ EVs, at first, two cell lines, SCC-9 and HaCaT, were employed as models. SCC-9 is a human tongue squamous cell carcinoma cell line with lymph node metastasis ability [25, 39, 40], while HaCaT is a type of human epithelial cell line commonly used to represent oral mucosal cells and is deemed to be lack of LNM capability [41]. It could be seen that SCC-9 secreted more $ASPH^+$ EVs than HaCaT, validated by nano-flow cytometry analysis and ELISA analysis (Figure S4). After pre-centrifuged to remove potential debris, the culture supernatant of these two types of cells was co-incubated with anti-ASPH modified microbeads for isolating $ASPH^+$ EVs. According to SEM images and corresponding NTA analysis (Figure S5A and B), it could be seen that more $ASPH^+$ EVs were captured on the surface of anti-ASPH modified microbeads as well as released for SCC-9 cells compared to HaCaT cells. Considering that ELISA was much more commonly-used in clinical laboratories in hospitals rather than NTA, we also implemented ELISA for analyzing the released $ASPH^+$ EVs from the immuno-microbeads, and the result was consistent with that of NTA (Figure S5C). Therefore, we could infer from all the above results that our microfluidic platform employing the immuno-microbeads as the core EV isolation component could effectively enrich $ASPH^+$ EVs and thus was able to distinguish cell lines with different LNM abilities.

Subsequently, clinical samples from 26 postoperative OSCC patients (13 with LNM and 13 without LNM, Table S1) were analyzed using this EV-based microfluidic LNM diagnosis strategy. At first, we analyzed the proportion of ASPH$^+$ PDF-EVs in both groups of patients with LNM and without LNM using nano-flow cytometry, and the results showed that the proportion of ASPH$^+$ PDF-EVs in the PDF of the LNM + group (6.58%) was higher than that of the LNM- group (3.39%) (Fig. 5A). However, ASPH$^+$ PDF-EVs of both groups counted less than 7% of the overall EV quantity in PDF, demonstrating that the isolation of ASPH$^+$ PDF-EVs was very difficult. Subsequently, PDF samples obtained from the patients were pre-centrifuged to remove large particles such as cells and debris and then were treated by our microfluidic platform. By imaging the anti-ASPH microbeads obtained from the microfluidic chips, as shown in Fig. 5B, it could be seen that there was significantly much more ASPH$^+$ PDF-EVs

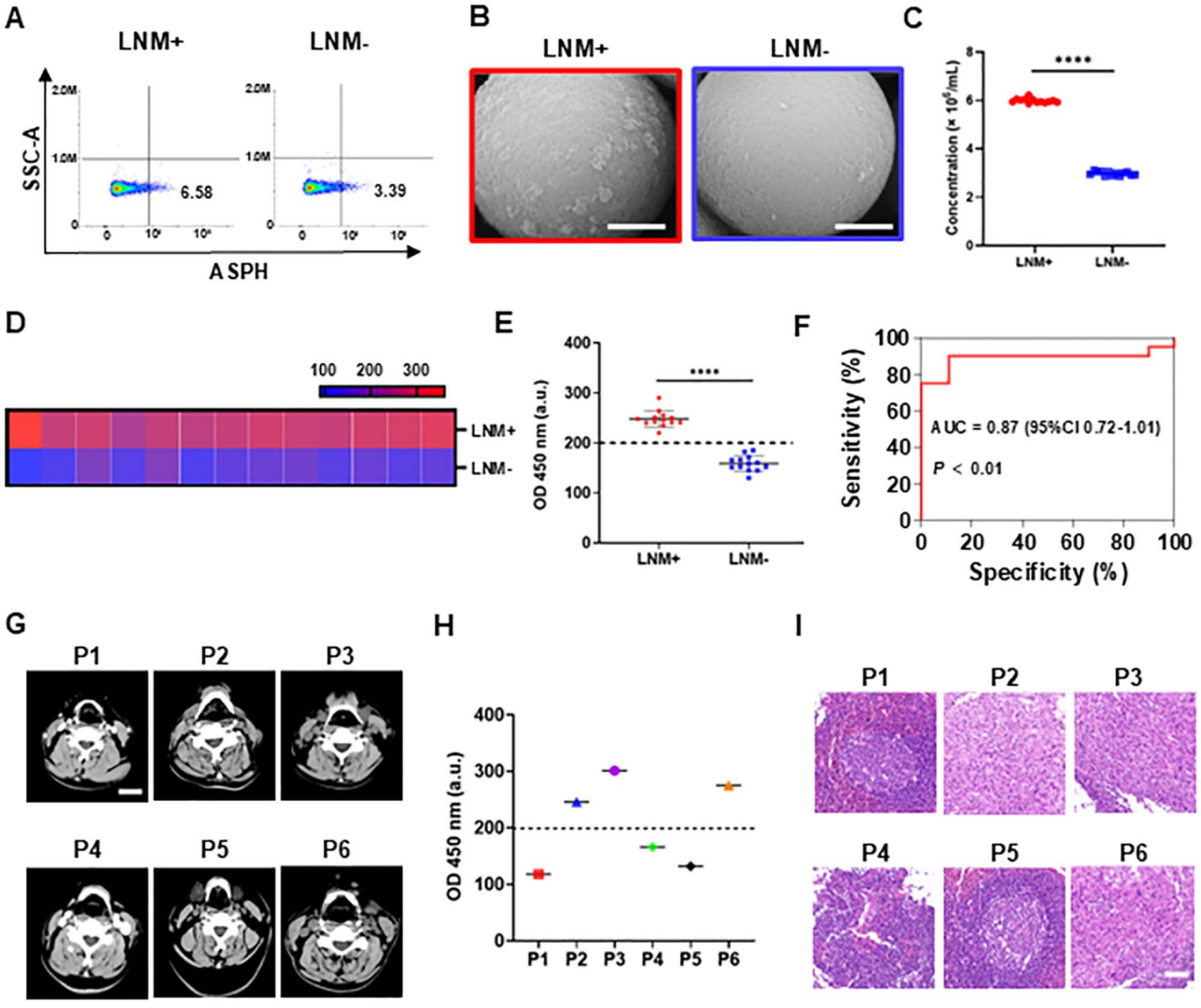

Fig. 5 Evaluation of the EV-based microfluidic strategy for LNM diagnosis for postoperative OSCC patients. (**A**) Nano-flow cytometry analysis comparing the level of ASPH$^+$ PDF-EVs between LNM + and LNM- OSCC patients. (**B**) SEM images showing anti-ASPH modified microbeads capturing ASPH$^+$ PDF-EVs from PDF of LNM + and LNM- OSCC patients. Scale bars, 2 μm. (**C**) NTA data showing the concentration of ASPH$^+$ PDF-EVs released from microfluidic chips treating PDF of 13 LNM + and 13 LNM- OSCC patients. (**D**) Heat maps of the OD value of ASPH$^+$ PDF-EVs from ELISA tests of the 13 LNM + and 13 LNM- patients. (**E**) Statistical analysis of the OD 450 nm value of ASPH$^+$ PDF-EVs from ELISA tests of the 13 LNM + and 13 LNM- patients, and OD (450 nm) value = 200 were determined as the threshold for defining LNM + and LNM-. (**F**) The AUC for the counts of ASPH$^+$ PDF-EVs between OSCC patients with and without LNM was 0.87, indicating an excellent diagnostic value (95% confidence interval: 0.72–1.01, $P < 0.01$). (**G**) Enhanced CT images of the neck of Patients 1–6 for blind tests. (**H**) The OD value of ASPH$^+$ PDF-EVs isolated in Patients 1–6 based on our strategy. (**I**) Pathological examination results of LN in Patient 1–6. Scale bar, 2 μm. ***$P<0.001$; ****$P<0.0001$. PDF, postoperative drainage fluid; ASPH, aspartate β-hydroxylase; EVs, extracellular vesicles; SEM, scanning electron microscope; LNM, lymph node metastasis; LN, lymph node; OSCC, oral squamous cell carcinoma; ELISA, enzyme-linked immunosorbent assay; AUC, area under the curve

captured by microbeads from OSCC patients with LNM compared to those without LNM. After releasing and retrieving the EVs from the microfluidic chips, the concentration of ASPH$^+$PDF-EVs was measured using NTA, and it was confirmed that the concentration of ASPH$^+$ PDF-EVs in the PDF of OSCC patients with LNM (about 6×10^6 /mL) was significantly higher than that of OSCC patients without LNM (about 3×10^6 /mL) (Fig. 5C). In order to facilitate the broad application of this EV-based microfluidic LNM diagnosis in clinical laboratories in hospitals, ELISA was demonstrated to quantitatively analyze the solutions containing ASPH$^+$ PDF-EVs released from those microfluidic chips, as shown in Fig. 5D **and E**. ELISA results also validated the higher ASPH protein expression in PDF-EVs from OSCC patients with LNM when comparing to those without LNM. In order to distinguish OSCC patients with / without LNM using ASPH$^+$ PDF-EVs as the indicator, we carefully analyzed the ELISA data and found that the OD 450 nm value of ASPH$^+$ PDF-EVs isolated in OSCC patients with LNM ranged from 220 to 290 (247.8 ± 16.4), while there were much less ASPH$^+$ PDF-EVs only ranging from 130 to 182 (158.6 ± 16.436) in OSCC patients without LNM. Furthermore, we conducted area under the curve (AUC) analysis (Fig. 5F). The AUC of the counts of ASPH$^+$ PDF-EVs between OSCC patients with and without LNM was 0.87, indicating that it had an excellent diagnostic value (95% confidence interval: 0.72–1.01, $P<0.01$). Therefore, we set the ASPH$^+$ PDF-EVs threshold for identifying OSCC with LNM as >200 based on our strategy to reflect the risk of LNM in postoperative OSCC patients. For validation, PDF samples from 6 OSCC patients (Table S2) were collected and blind tested using our strategy. At the very beginning, none of the 6 patients was found to have LNM according to imaging examinations (Fig. 5G). Subsequently, their PDF was collected and analyzed by the EV-based microfluidic diagnosis strategy and results showed that the OD (450 nm) value of ASPH$^+$ PDF-EVs from Patient 1, 4 and 5 were less than 200 (118, 166 and 132, respectively), while the PDF of Patient 2, 3 and 6 contained more ASPH$^+$ PDF-EVs (OD (450 nm) value=246, 301 and 275, respectively) (Fig. 5H), indicating a higher risk of LNM for Patient 2, 3 and 6. Finally, pathological analysis from their surgical excision confirmed the presence of LNM in Patient 2, 3 and 6 rather than Patient 1, 4 and 5 (Fig. 5I). This blind test demonstrated the potential ability of our ASPH$^+$ PDF-EVs based microfluidic strategy for accurate detection of LNM in postoperative OSCC patients in clinical practices.

Conclusion

Fast diagnosis of LNM for postoperative OSCC patients can benefit the timely treatment and improve prognosis. In this work, we developed a strategy quickly diagnosing LNM in OSCC patients after neck dissection by isolation, purification, release and purification of ASPH$^+$ PDF-EVs based on a microfluidic cascade. In previous clinical practices, PDF was always considered as medical waste and its value as an indicator of disease progression has been neglected for a long time. Our study used microfluidic technology to analyze specific EVs inside the PDF after neck dissection for the first time and demonstrated the promise of ASPH$^+$ PDF-EVs as a new kind of liquid biopsy indicating LNM in OSCC. And by using multiple microfluidic chips as a cascade, ASPH$^+$ PDF-EVs are expected to be analyzed to enable fast diagnosis with higher precision or sensitivity. We believe that this platform will help guide the precise treatment of patients with LNM in OSCC and formulate treatment strategies for patients with different LNM risk levels. Furthermore, we also expect the technique will help promote the preservation of lymph nodes in OSCC patients and finally improve their survival and quality of life.

Abbreviations

LNM	Lymph node metastasis
OSCC	Oral squamous cell carcinoma
EVs	Extracellular vesicles
PDF	Postoperative drainage fluid
ASPH	Aspartate β-hydroxylase
ELISA	Enzyme-linked immunosorbent assay
EpCAM	Epithelial cell adhesion molecule
GEPIA	Gene Expression Profiling Interactive Analysis
TCGA	The Cancer Genome Atlas
LC-MS	Liquid chromatography-mass spectrometry
SiO_2	Silica
MPTMS (3-mercaptopropyl)	Trimethoxysilane
GMBS	4-maleimidobutyric acid N-hydroxysuccinide ester
SA	Streptavidin
SEM	Scanning electron microscope
TEM	Transmission electron microscope
NTA	Nanoparticle tracking analysis
DMSO	Dimethylsulfoxide
DLS	Dynamic light scattering
BSA	Bovine serum albumin
AUC	Area under the curve

Supplementary Information

The online version contains supplementary material available at https://doi.org/10.1186/s12951-024-02846-1.

Supplementary Material 1

Supplementary Material 2

Acknowledgements

This study was funded by Postdoctoral Science Foundation of China (2018M630883 & 2019T120688), Fundamental Research Funds for the Central Universities ("Medicine + X") (2042024YXB017), Hubei Province Chinese Medicine Research Project (ZY2023Q015), Natural Science Foundation of China (61904057 and 22193051) and Natural Science Foundation of Hubei Province (2018CFB124), Youth Interdisciplinary Special Fund of Zhongnan Hospital of Wuhan University (ZNQNJC2022003), the Medical Young Talents Program of Hubei Province and Wuhan Young Medical Talents Training Project.

Author contributions
Zi-Zhan Li: Conceptualization, Methodology, Investigation, Writing - Original Draft, Visualization. Nian-Nian Zhong, Guang-Rui Wang, Yao Xiao: Methodology, Investigation, Formal analysis, Visualization. Lei-Ming Cao, Zhao-Qi Zhu and Xuan-Hao Liu: Methodology, Investigation, Visualization. Ze-Min Cai: Methodology, Investigation, Formal analysis, Writing - Original Draft. Wen-Tao Zhu and Ke Wu: Methodology, Investigation. Rong-Xiang He and Xing-Zhong Zhao: Writing - Review & Editing. Bing Liu, Bo Cai and Lin-Lin Bu: Conceptualization, Methodology, Writing - Review & Editing, Project administration, Funding acquisition. All authors reviewed and approved the final manuscript.

Data availability
The authors declare that they have no known competing financial interests or personal relationships that could have appeared to influence the work reported in this paper.

Declarations

Competing interest
The authors declare that they have no known competing financial interests or personal relationships that could have appeared to influence the work reported in this paper.

Author details
[1]State Key Laboratory of Oral & Maxillofacial Reconstruction and Regeneration, Key Laboratory of Oral Biomedicine Ministry of Education, Hubei Key Laboratory of Stomatology, School & Hospital of Stomatology, Wuhan University, Wuhan 430079, Hubei, China
[2]Hubei Key Laboratory of Environmental and Health Effects of Persistent Toxic Substances, School of Environment and Health, Jianghan University, Wuhan 430056, China
[3]School of Electronic and Electrical Engineering, Wuhan Textile University, Wuhan 430200, China
[4]Department of Oral & Maxillofacial - Head Neck Oncology, School & Hospital of Stomatology, Wuhan University, Wuhan 430079, Hubei, China
[5]School of Physics and Technology, Wuhan University, Wuhan 430072, China

Received: 15 July 2024 / Accepted: 7 September 2024
Published online: 28 September 2024

References

1. Ch'ng ES. Head and Neck Cancer. N Engl J Med. 2020;382(20):e57.
2. Leemans CR, Braakhuis BJ. Brakenhoff the molecular biology of head and neck cancer. Nat Rev Cancer. 2011;11(1):9–22.
3. Wang W, Adeoye J, Thomson P. Choi multiple tumour recurrence in oral, head and neck cancer: characterising the patient journey. J Oral Pathol Med. 2021;50(10):979–84.
4. Warnakulasuriya S. Kerr oral Cancer screening: past, Present, and Future. J Dent Res. 2021;100(12):1313–20.
5. Shanti RM, O'Malley BW. Jr Surg Manage Oral Cancer Dent Clin North Am. 2018;62(1):77–86.
6. Chang TG, Huang PC, Hsu CY. Yen demoralization in oral cancer inpatients and its association with spiritual needs, quality of life, and suicidal ideation: a cross-sectional study. Health Qual Life Outcomes. 2022;20(1):60.
7. Sarode GS, Sengupta N, Yuwanati M, Gondivkar S, Gadbail A, Upadhyay P. Sarode Perspective on the risk of suicide associated with oral cancer diagnosis. Future Oncol. 2022;18(35):3863–5.
8. Gotze H, Friedrich M, Taubenheim S, Dietz A, Lordick F. Mehnert Depression and anxiety in long-term survivors 5 and 10 years after cancer diagnosis. Support Care Cancer. 2020;28(1):211–20.
9. Okati-Aliabad H, Ansari-Moghadam A, Mohammadi M, Kargar S. Shahraki-Sanavi the prevalence of anxiety and depression and its association with coping strategies, supportive care needs, and social support among women with breast cancer support. Care Cancer. 2022;30(1):703–10.
10. Wang GR, Wang HQ, Zhong NN, Cao LM, Li ZZ, Liu XH, Xiao Y, Liu B. Bu suicide among patients with oral cancer: a population-based study. Cancer Epidemiol. 2024;92:102625.
11. Li ZZ, He JY, Wu Q, Liu B. Bu recent advances in targeting myeloid-derived suppressor cells and their applications to radiotherapy. Int Rev Cell Mol Biol. 2023;378:233–64.
12. Wang KN, Li ZZ, Cai ZM, Cao LM, Zhong NN, Liu B, Zhou K, Huo FY, Cai B. L.L. Bu the applications of flexible electronics in dental, oral, and craniofacial medicine Npj. Flex Electron 2024;8(1).
13. Cai ZM, Li ZZ, Zhong NN, Cao LM, Xiao Y, Li JQ, Huo FY, Liu B, Xu C, Zhao Y, Rao L. Bu revolutionizing lymph node metastasis imaging: the role of drug delivery systems and future perspectives. J Nanobiotechnol. 2024;22(1):135.
14. Li ZZ, Zhong NN, Cao LM, Cai ZM, Xiao Y, Wang GR, Liu B, Xu C. L.L. Bu nanoparticles Targeting Lymph nodes for Cancer Immunotherapy: strategies and Influencing Factors Small 2024;e2308731.
15. Xu ZY, Li ZZ, Cao LM, Zhong NN, Liu XH, Wang GR, Xiao Y, Liu B. L.L. Bu seizing the fate of lymph nodes in immunotherapy: to preserve or not? Cancer Lett 2024;216740.
16. Wu S, Hong G, Xu A, Zeng H, Chen X, Wang Y, Luo Y, Wu P, Liu C, Jiang N, Dang Q, Yang C, Liu B, Shen R, Chen Z, Liao C, Lin Z, Wang J. Lin Artificial intelligence-based model for lymph node metastases detection on whole slide images in bladder cancer: a retrospective, multicentre, diagnostic study. Lancet Oncol. 2023;24(4):360–70.
17. Zhong NN, Wang HQ, Huang XY, Li ZZ, Cao LM, Huo FY, Liu B. Bu Enhancing head and neck tumor management with artificial intelligence: integration and perspectives Semin. Cancer Biol. 2023;95:52–74.
18. Alix-Panabieres C, Magliocco A, Cortes-Hernandez LE, Eslami SZ, Franklin D. Messina Detection of cancer metastasis: past, present and future Clin. Exp Metastasis. 2022;39(1):21–8.
19. Ashktorab H. Brim blood-based liquid biopsies: a noninvasive and cost-effective Tool for Improved Risk Assessment and Identification of Lymph Node Metastasis in patients with Submucosal T1 colorectal. Cancer Gastroenterol. 2021;161(1):29–31.
20. Xue L, Zhao Z, Wang M, Ma L, Lin H, Wang S, Xue X, Liu L, Wang B, Li Z, Yang Z, Lu N, Zhan Q. Song a liquid biopsy signature predicts lymph node metastases in T1 oesophageal squamous cell carcinoma: implications for precision treatment strategy. Br J Cancer. 2022;127(11):2052–9.
21. Asakura K, Matsuzaki J. Ochiya Liquid biopsy in lung cancer: a surgical perspective. Cancer Sci. 2023;114:16–16.
22. Egunov AI, Dou Z, Karnaushenko DD, Hebenstreit F, Kretschmann N, Akgun K, Ziemssen T, Karnaushenko D, Medina-Sanchez M. Schmidt Impedimetric Microfluidic Sensor-in-a-Tube for label-free. Immune Cell Anal Small. 2021;17(5):e2002549.
23. Kalluri R, McAndrews KM. role Extracell Vesicles cancer Cell. 2023;186(8):1610–26.
24. Xiong H, Huang Z, Yang Z, Lin Q, Yang B, Fang X, Liu B, Chen H. J Kong Recent Progress Detect Profiling Cancer Cell-Derived Exosomes Small. 2021;17(35):e2007971.
25. Wang J, Man QW, Fu QY, Zhong NN, Wang HQ, Li SR, Gao X, Lin H, Su FC, Bu LL, Chen G. Liu Preliminary Extracellular Vesicle Profiling in Drainage Fluid after Neck Dissection in OSCC. J Dent Res. 2023;102(2):178–86.
26. Candau-Alvarez A, Linares-Sicilia MJ, Dean-Ferrer A, Br. J Oral Maxillofac Surg. 2015;53(2):200–3.
27. Yan W. Jiang Immune Cell-Derived exosomes in the Cancer-Immunity cycle. Trends Cancer. 2020;6(6):506–17.
28. Rao KU. Godaly isolation and purification of mycobacterial extracellular vesicles (EVs). Methods Mol Biol. 2023;2674:55–60.
29. Hart CD, Galardi F, Pestrin M, De Luca F, Risi E. Di Leo Using CTCs Pharmacogenomic Anal Pharmacol Res. 2016;106:92–100.
30. Gwak H, Park S, Yu H, Hyun K.A., Jung H.I. A modular microfluidic platform for serial enrichment and harvest of pure extracellular vesicles. Analyst. 2022;147(6):1117–27.
31. Wang J, Ma P, Kim DH, Liu B-F. Demirci towards microfluidic-based exosome isolation and detection for tumor therapy. Nano Today. 2021;37:101066.
32. Yang F, Liao X, Tian Y. Li Exosome separation using microfluidic systems: size-based, immunoaffinity-based and dynamic methodologies. Biotechnol J. 2017;12(4):1600699.
33. Lin Q, Chen X, Meng F, Ogawa K, Li M, Song R, Zhang S, Zhang Z, Kong X, Xu Q, He F, Liu D, Bai X, Sun B, Hung MC, Liu L, Wands JR. Dong multi-organ metastasis as destination for breast cancer cells guided by biomechanical architecture. Am J Cancer Res. 2021;11(6):2537–67.
34. Kanwal M, Smahel M, Olsen M, Smahelova J. R. Tachezy Aspartate β-hydroxylase as a target for cancer therapy. J Exp Clin Canc Res 2020;39(1).

35. Zhou K, Li ZZ, Cai ZM, Zhong NN, Cao LM, Huo FY, Liu B, Wu QJ. Bu Nanotheranostics in cancer lymph node metastasis: the long road ahead. Pharmacol Res. 2023;198:106989.
36. Garcia-Ceron D, Dawson CS, Faou P, Bleackley MR. Anderson size-exclusion chromatography allows the isolation of EVs from the filamentous fungal plant pathogen Fusarium oxysporum f. sp. vasinfectum (Fov. Proteomics. 2021;21(13–14):e2000240.
37. Huang Q, Cai B, Chen B, Rao L, He Z, He R, Guo F, Zhao L, Kondamareddy KK, Liu W, Guo S. Zhao efficient purification and release of circulating Tumor cells by Synergistic Effect of Biomarker and SiO2@Gel-Microbead-Based size difference amplification Advanced. Healthc Mater. 2016;5(13):1554–9.
38. Wei X, Ao Z, Cheng L, He Z, Huang Q, Cai B, Rao L, Meng Q, Wang Z, Sun Y, Liu W, Zhang Y, Guo S, Guo F, Zhao X.-Z. Highly sensitive and rapid isolation of fetal nucleated red blood cells with microbead-based selective sedimentation for non-invasive prenatal diagnostics. Nanotechnology. 2018;29(43):434001.
39. Agostini M, Almeida LY, Bastos DC, Ortega RM, Moreira FS, Seguin F, Zecchin KG, Raposo HF, Oliveira HC, Amoedo ND, Salo T, Coletta RD. Graner the fatty acid synthase inhibitor orlistat reduces the growth and metastasis of orthotopic tongue oral squamous cell carcinomas. Mol Cancer Ther. 2014;13(3):585–95.
40. Busso-Lopes AF, Carnielli CM, Winck FV, Patroni FMS, Oliveira AK, Granato DC, RAP EC, Domingues RR, Pauletti BA, Riano-Pachon DM, Aricetti J, Caldana C, Graner E, Coletta RD, Dryden K, Fox JW. Paes Leme A Reductionist Approach using primary and metastatic cell-derived extracellular vesicles reveals Hub proteins Associated with oral. Cancer Prognosis Mol Cell Proteom. 2021;20:100118.
41. Gould SJ, Foey AD. Salih an organotypic oral mucosal infection model to study host-pathogen interactions. J Tissue Eng. 2023;14:20417314231197310.

Publisher's note